HTD-Vol. 364-4, Proceedings of the ASME
Heat Transfer Division — 1999
Volume 4
ASME 1999

PERFORMANCE AND MODELING OF HEAT FLUX SENSORS IN DIFFERENT ENVIRONMENTS

D. G. Holmberg
C. A. Womeldorf

Building and Fire Research Laboratory
National Institute of Standards and Technology
Gaithersburg, MD

ABSTRACT

Heat flux measurement is not simple; care is required in selecting a suitable sensor for a given application. Surface substrate properties and the convective and radiative environment determine the choice of sensors. Mounting of the sensor, especially in calibration versus application, influences accuracy of measurement. The purpose of the present study is to increase awareness of potential errors in heat flux sensor use. This paper compares sensor performance in general by examining results of testing three commercially available sensors and by numerical modeling of these sensors. Comparisons of sensor calibrations in the NIST convective heat flux calibration facility are made with manufacturer calibrations and give evidence of potential pitfalls when using a sensor in a different environment than the calibration environment. Modeling results help explain observed data, demonstrating specific sensor parameters that can lead to significantly different calibrations in different environments.

NOMENCLATURE

k	Thermal conductivity (W/mK).
q''_{ref}	Reference heat flux in convective facility (W/cm^2)
q''_{sens}	Flux normal to sensor surface, $k \cdot \Delta T/x$ in numerical model, where ΔT is the temperature difference between two nodes separated by a vertical distance x.
$q''_{sens\ actual}$	Estimated flux leaving the sensor surface for a sensor mounted in the calibration facility.
q''_{sub}	Flux to substrate surface.
$q''_{inc\ rad}$	Incident radiation, σT_{source}^4.
$q''_{abs\ rad}$	Radiation flux that is absorbed at the surface, $\varepsilon_{sens}\,\sigma\,(T_{source}^4 - T_{sens}^4)$.
q''_{conv}	Convective heat flux, $h\,\Delta T_{flow}$, where h is the heat transfer coefficient.
ΔT_{flow}	Convective temperature difference for calibration facility, $T_{plate} - T_{air}$ (K)
ε	Total hemispherical emissivity.

INTRODUCTION

Heat flux measurement is performed with a variety of sensors, both off-the-shelf as well as custom made. Most sensors are calibrated in a radiation field with black paint on the sensor surface, but often used in combined radiation and convection environments, and often mounted differently in the application environment. These differences can lead to large errors in measured heat flux.

An initiative was begun in FY1995 at the National Institute of Standards and Technology (NIST) to develop three heat flux sensor calibration facilities to allow independent heat flux sensor calibration in radiation, convection, and conduction. These facilities have been presented in Murthy *et. al.* (1997), Holmberg and Womeldorf (1998, 1999), and Grosshandler and Blackburn (1997).

The NIST radiation and convection calibration references are considerably different. The radiation calibration is performed with the sensor located precisely relative to a radiation source of known intensity, so that the *incident* flux is known with high precision. This is the radiation heat flux reference. A commercial sensor is usually calibrated in a radiation environment (e.g. exposed to a hot lamp) using a transfer standard calibrated in the NIST (or equivalent) radiation facility.

The NIST convection calibration facility is a low-speed open wind tunnel with a 30:1 2-D contraction entering a 300mm wide by 10 mm high test section. Air flows over the constant-temperature guarded hot plate in which the reference and sensor are mounted, Fig. 1. The boundary layer is laminar across the sensor with slot height Re_h = 20,000. Unlike the radiation calibration, the heat source in the NIST convection calibration facility is the calibration plate in which the sensor is mounted with flux from the hot plate to the cool air flowing over it. The calibration reference is a carefully guarded region of the plate with flux equal to the reference power divided by its area, with this reference at the same downstream location as the sensor under calibration (Fig. 1). The reference is not an incident radiative flux, but the *flux that would pass through the plate surface if no sensor were present*. The flux through the sensor itself may be different due to the

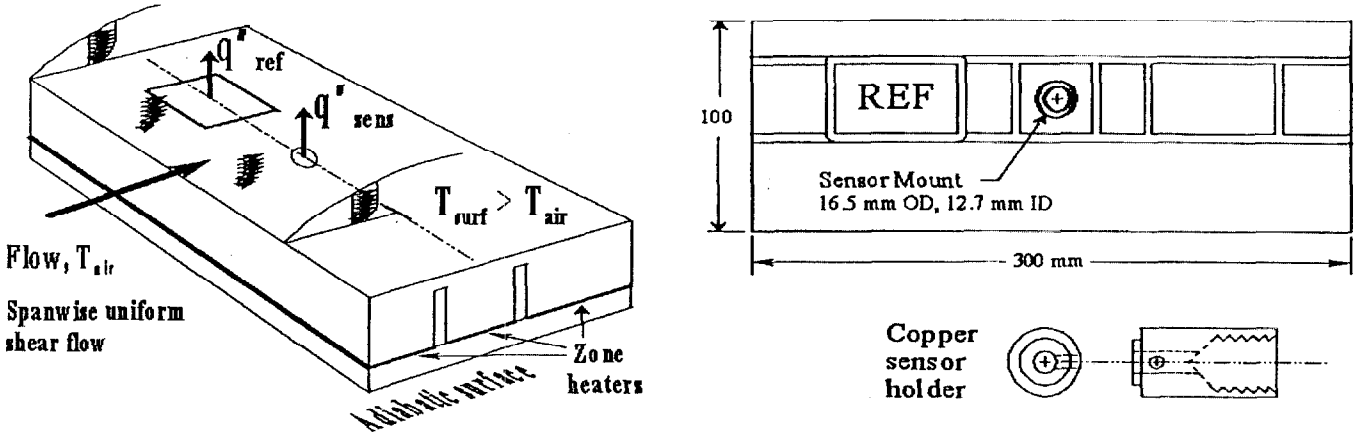

Figure 1 Schematic of convection calibration plate (left) showing comparison of reference and sensor fluxes at same downstream location on plate. Bottom view of plate (right) shows sensor mounting hole. Sensor holder (this one used for sensor S1) inserts in mounting hole.

sensor's presence altering the convective and radiative fluxes relative to the surrounding (reference) surface, Fig. 2. However, the desired calibration is the flux through the surrounding surface as a function of sensor output.

The purpose of this paper is to demonstrate the potential for error in heat flux measurement due to differences between a sensor's calibration and application environments. The performance of three sensors in the NIST convective calibration facility is compared with manufacturer calibrations. Sources of error are discussed and numerical modeling performed to demonstrate relative significance of various error sources. These data are meant to show the limitations of a sensor calibration. The cases presented here are not meant to be exhaustive but rather to allow the reader to understand the pitfalls in heat flux sensor calibration and heat flux measurement.

ERROR SOURCES IN CALIBRATION AND APPLICATION

The typical calibration is given as sensor voltage output versus incident radiation, Fig. 3. Alternatively, an absorbed flux calibration may be given, where the absorbed flux is commonly taken as the incident flux multiplied by the emissivity, neglecting re-radiated energy (emitted, Fig. 3). Other possible calibrations are those obtained in the NIST convection facility or conduction facility which minimize radiation in the calibration environment, giving calibrations ideally equivalent to the radiation absorbed flux calibration. As will be seen, changing the boundary conditions by which the flux is applied can change the achieved calibration. What is not generally understood is the degree of sensitivity of these calibrations to the particular sensor design, thermal properties, surface condition, and mounting in calibration versus application.

Error sources can be categorized according to the following: sensor/substrate differences (surface and material thermal properties), internal sensor design, and mounting. For incident radiation measurements with cooled sensors, sensor/substrate differences are not an issue as long as the sensor is completely isolated from the surrounding substrate in both calibration and application. Measures must be taken to ensure that the mounting in calibration versus application does not influence the flow of energy through the sensor. For example, a cold sensor calibrated in a cold copper sleeve will not be largely influenced by the presence of the sleeve even though in contact. However, if the same sensor is mounted in good contact with a hot wall, the cold sensor will absorb energy from the wall laterally, which can significantly alter the calibration. In addition, any convection present in the application environment will add to (or subtract from) the desired radiant flux.

When seeking the undisturbed (no sensor present) flux to a

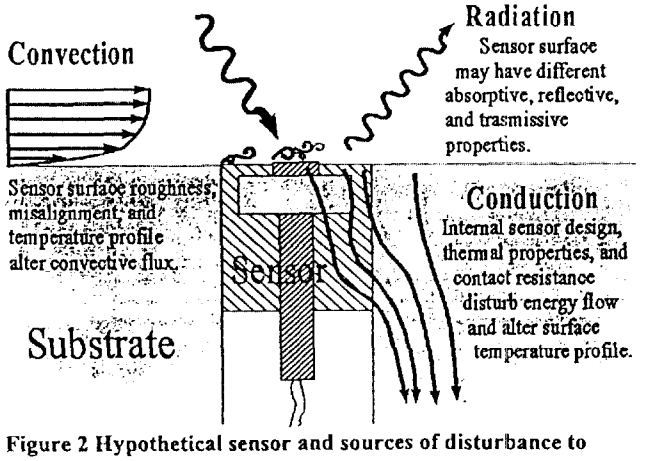

Figure 2 Hypothetical sensor and sources of disturbance to convective and radiative fluxes.

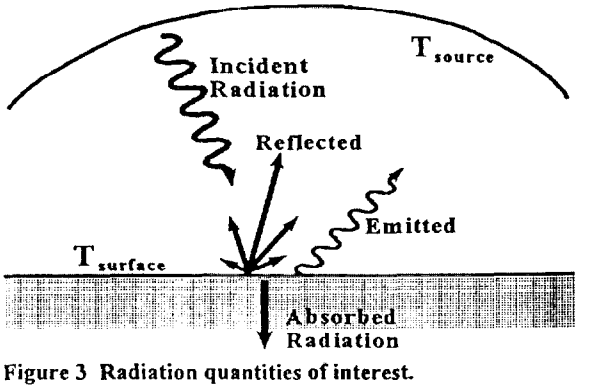

Figure 3 Radiation quantities of interest.

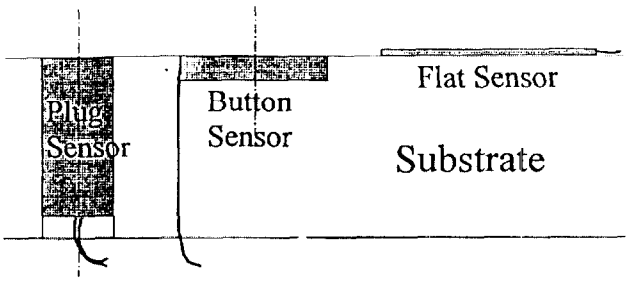

Figure 4 Schematic of three sensors: test mounting and modeling configuration.

surface, matching sensor to substrate properties is key. Second to this is minimizing contact resistance. If a low conductivity sensor is mounted in a high conductivity substrate, the sensor will become a hot-spot (assuming flux direction is into the surface). This overheat (temperature rise) will result in under-reporting of convective flux if the overheat is significant relative to the temperature difference between the flow and surface. The hot sensor will also affect the boundary layer and may result in significant change to the local heat transfer coefficient (Kim *et. al.*, 1996). If the overheat is large enough, it can also be significant relative to the temperature difference between the radiation source and substrate surface. For such a high overheat the convection can actually end up cooling the sensor. Given sensor overheat, even if the same sensor were calibrated at the same flux level mounted in the same way in the same substrate, but calibrated in radiation, this calibration would not be valid in a convective application.

Given matched sensor and substrate thermal conductivity, surface emissivity also must be matched to accurately measure radiation. If convection is present, then surface roughness and any discontinuity (sensor not flush with surface) must be considered (Fig. 2). Given a sensor that matches the surrounding substrate, it is still possible to have significant error if the sensor is not mounted with negligible contact resistance. If a sensor is mounted with some contact resistance (e.g. air gap) then it will have some overheat with the problems discussed above. Likewise, if a sensor is calibrated with contact resistance present, but installed such that the contact resistance is more or less, error can result.

Lastly, internal sensor design can affect the degree to which a given sensor responds differently to these variables. A differential thermopile consisting of multiple thermocouples in series wrapped around some resistance layer can be very sensitive to lateral flux (due to mismatch of substrate and sensor) if the thermopile extends across a large part of the vertical dimension of the sensor, since there is opportunity for energy to enter via the side and increase the flux seen by the thermopile even though that flux is not present at the sensor surface. Conversely, a very thin thermopile at the surface will not be significantly influenced. In addition, the presence of lower thermal conductivity elements (epoxy potting, air spaces, resistance layers, glue layers), can alter conduction through the sensor relative to the surrounding substrate.

These factors all can contribute to very large errors in measurement of heat flux. The following section presents calibration data for three sensors comparing manufacturer calibration to calibration in the NIST convection calibration facility. An explanation is given attempting to reconcile these different calibrations, followed by numerical modeling of these sensors to help explain observed results and illustrate some of the points discussed above.

TEST SENSOR DESCRIPTIONS

The three sensors tested here, Fig. 4, are all similar in that they measure heat flux directly using a thermopile consisting of copper-constantan differential thermocouples connected in series across a thermal resistance layer. General methods for measuring heat flux are reviewed in Diller (1993, 1998), and Keltner (1997). The sensors vary in their bulk thermal conductivity, thickness of the thermal resistance layer, surface emissivity, mounting method, and shape of the sensor body. Further sensor details are given in Table 1.

Sensor one (Plug) is a Schmidt-Boelter type sensor (Kidd and Nelson, 1995). The thermal resistance element is embedded in a 6.4 mm diameter, 16 mm long copper cylindrical housing with leads exiting out the back. Typically, this type of sensor is used in a mixed convective and radiative environment at high flux levels, and calibrated in radiation.

Sensor two (Button) has a thermal resistance layer and body of lower thermal conductivity polymer resin in the shape of a disk, 9.3 mm diameter, 1.8 mm thick. A type-T thermocouple is embedded in the body. The copper leads exit from the side of the disk. This sensor is typically used in low flux applications, and calibrated in radiation.

Sensor three (Flat) is a flexible polyimide sensor with sensor thickness of 0.08 mm, and sensor area of 15 x 15 mm. A type-T

Table 1 Test sensor specifications.

	Plug Sensor	*Button Sensor*	*Flat Sensor*
Heat flux sensor type	Schmidt-Boelter; differential thermopile	Polymer disk; differen. thermopile	Polyimide thin-film; differential thermopile
Manuf. supplied cal	9.26 $^{mV}/_{W/cm2}$	18.10 $^{mV}/_{W/cm2}$	4.05 $^{mV}/_{W/cm2}$ with curve to correct for temp.
Manuf. cal method	Radiation versus transfer standard	Radiation vs. transfer standard	Conduction versus transfer standard
Design heat flux	11.4 W/cm^2 max	1.26 W/cm^2 max	Not specified
Temperature limits	T < 200C recommended, 330C max	150 C	Not given.
Internal construction	Wire-wound wafer potted in copper cylinder using epoxy.	Phenolic resin thermal resistance layer molded in epoxy body.	Foil thermopile across polyimide resistance layer sandwiched by polyimide.
Bulk thermal cond	200 W/mK (epoxy potting much lower)	0.43 W/mK	0.14 W/mK
Body dimensions	6.35 mm diam cylinder, 16 mm long	9.3 mm diam disk, 1.8 mm thick	Active area 15mm x 15mm, 0.075 mm thick.
Surface coating	High emiss black paint, $\varepsilon = 0.96$	High emiss black paint, $\varepsilon = 0.94$	No coating; polyimide $\varepsilon = 0.6$
Mounting details	Sliding fit in hole with set screw; flush with surface.	Set in countersunk hole with glue, flush with surface.	Fixed to surface with 0.05 mm thick sheet of wax, T_{melt} = 113 C
Thermocouple	None	Type T, 30 awg	Type T, foil
Typical Applications	High flux aerodynamic	Biomedical, low flux	Low flux

thermocouple is located beside the heat flux sensor, [illegible] the four foil copper leads exit out the side. This sensor is calibrated in conduction.

Each sensor was calibrated in the convection facility using the first-generation calibration plate. The calibration flux is from the heated plate surface to a cool air flow. The reference is not incident radiant flux, but rather the electrical power required to heat the reference area, which gives the actual flux at the reference. The flux through the test sensor surface is not equal to the reference flux due to the disturbance of the sensor itself, with test sensor surface temperature deficit and radiation characteristics the main differences. The first-generation plate has an estimated emissivity (lightly oxidized polished copper) of 0.1. This value has been used to estimate the radiation from the plate reference to the unheated upper test section surface. The calibration reference heat flux reported here will be only the convection component after removing the radiation.

Plug Sensor Calibration

The Plug sensor was delivered to NIST with a responsivity calibrated versus incident radiation equal to 9.26 $^{mV}/_{W/cm2}$, with a manufacturer estimated uncertainty of ± 3 % at 4:1 odds (equivalent to ± 5 % at 95 % level of confidence) and with a stated surface emissivity of 0.96.

Subsequently the plug sensor was calibrated in the NIST radiation facility (Murthy, *et. al.*, 1997) resulting in a responsivity of 8.71 $^{mV}/_{W/cm2}$ ± 2 % (95 % level of confidence). Since both measure incident radiation, these two calibrations should agree. However, it was later determined that the paint on the sensor surface had changed appearance. It was no longer flat black, but instead had an oily appearance (likely from handling with fingers). Oil can significantly increase the reflectance of the sensor and reduce absorbed flux, lowering the responsivity as seen.

The plug sensor was then calibrated in the NIST convection facility. The sensor was mounted in the calibration plate and held in a copper sensor holder (Fig. 1). Electrical resistance heaters attached to the calibration plate supply heat that is conducted to the sensor holder and then to the sensor. Thermal grease is used to reduce contact resistance between these parts, but some drop in temperature at the sensor surface occurs which results in a lower convective flux relative to the flux at the reference.

Calibration results are presented in Table 2. The reference convective flux and sensor ouput are given for eight data points. The average responsivity from the convection testing is 9.91 $^{mV}/_{W/cm2}$ with an uncertainty on the reference flux of 4.6 % (relative combined uncertainty, Holmberg and Womeldorf, 1999). This calibration is equivalent to a total absorbed flux calibration, rather than an incident flux calibration. Taking the original manufacturer calibration of 9.26 $^{mV}/_{W/cm2}$ and translating to an absorbed flux calibration by dividing by emissivity (0.96) gives a calibration coefficient of 9.65 $^{mV}/_{W/cm2}$.

The last column of Table 2 gives responsivity of the sensor based on the estimated flux actually leaving the sensor surface, rather than the convective reference. This flux includes the sensor radiative component (12% of the total flux from the sensor at ΔT_{flow} = 80 K) and accounts for a slightly cooler sensor surface due to contact resistance around the sensor and thermal resistance within the sensor. Surface temperature estimates were made based on liquid crystal surface temperature visualization tests. The estimated additional uncertainties on surface temperature and surface emissivity have been combined with the convection reference uncertainty to yield the 7.5% value (column bottom). The resulting 9.55 $^{mV}/_{W/cm2}$ value is very close

Table 2 Plug sensor calibration results

ΔT_{flow} (T_{plate}-T_{air}) (K)	q''_{ref} convective (W/cm²)	Sensor output (mV)	Responsiv. (q''_{ref}) (mV/W/cm²)	Responsivity (est. $q''_{sens,actual}$) (mV/W/cm²)
19.91	0.1138	1.09	9.61	9.42
40.17	0.2317	2.27	9.79	9.52
40.29	0.2320	2.26	9.75	9.48
59.8	0.3372	3.44	10.21	9.82
59.85	0.3468	3.42	9.86	9.51
60.08	0.3370	3.41	10.12	9.72
79.93	0.4658	4.64	9.96	9.51
98.98	0.5800	5.80	10.00	9.46
	Average responsivity		*9.91*	*9.55*
	Uncertainty (2 sd) on flux		*4.6 %*	*7.5 %*

to the manufacturer calibration (absorbed flux) of 9.65 $^{mV}/_{W/cm2}$ and demonstrates good agreement between the manufacturer radiation calibration and the NIST convection calibration.

Button Sensor Calibration

The button sensor was delivered to NIST with an incident radiation responsivity of 18.10 $^{mV}/_{W/cm2}$ and no stated uncertainty, and with emissivity of 0.94. Manufacturer calibration was performed in radiation versus a transfer standard. No radiation calibration was performed at NIST.

For the convection calibration, the sensor was glued into a hole countersunk in the face of a copper cylinder that was mounted into the calibration plate as shown in Fig. 5. This allowed the sensor to be set flush with the calibration plate surface to have minimal flow disruption over the sensor and good thermal contact with the flat bottom of the sensor. As with the plug sensor, heating of the sensor was via conduction from the surrounding calibration plate, resulting in a sensor colder than the plate.

Calibration results are presented in Table 3 with an average responsivity, based on the reference convective flux, of 10.42 $^{mV}/_{W/cm2}$. This is approximately half the output expected based on the manufacturer calibration. With an analysis similar to that for the plug sensor, considering surface temperature and radiation, this discrepancy can only be partially explained. In addition to the contact resistance related to the double cylinder sensor holder arrangement (Fig. 5), the

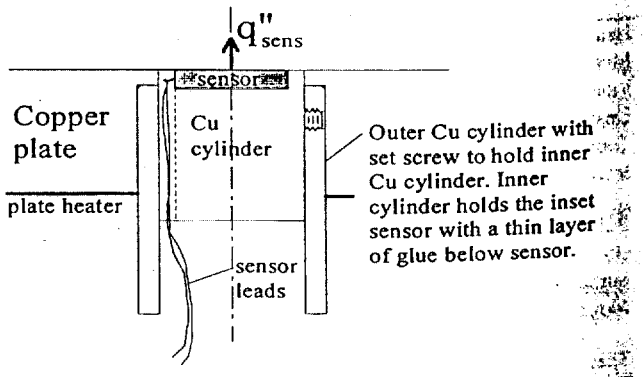

Figure 5 Button sensor installation in convection calibration plate.

Table 3 Button sensor calibration results

ΔT_{flow} (T_{plate}-T_{air}) (K)	q''_{ref} convective (W/cm^2)	Sensor output (mV)	Responsiv. (q''_{ref}) ($mV/W/cm^2$)	Responsivity (est. $q''_{sens,actual}$) ($mV/W/cm^2$)
19.37	0.1143	1.126	9.85	12.02
39.59	0.2322	2.401	10.34	12.48
40.07	0.2322	2.429	10.46	12.47
79.08	0.4658	5.13	11.01	13.19
	Average responsivity		***10.42***	***12.54***
	Uncertainty (2 sd) on flux		***4.6 %***	***6.5 %***

Table 4 Flat sensor calibration results

ΔT_{flow} (T_{plate}-T_{air}) (K)	q''_{ref} convective (W/cm^2)	Sens output (linearized) (mV)	Responsiv. (q''_{ref}) ($mV/W/cm^2$)	Responsiv. ($q''_{sens,actual}$) ($mV/W/cm^2$)
19.89	0.1151	0.477	4.10	3.98
40.20	0.2337	0.994	4.20	4.08
59.71	0.3491	1.500	4.24	4.11
79.83	0.4686	2.045	4.30	4.16
	Average responsivity		***4.21***	***4.08***
	Uncertainty (2 sd) on flux		***4.6 %***	***5.0 %***

sensor thermal conductivity (k_{bulk} = 0.43 W/mK from manufacturer) is very low relative to the copper plate, limiting heat transfer through itself and causing a significant temperature drop (25% of ΔT_{flow}) at the surface of the sensor relative to the surrounding plate. These factors reduce the flux through the sensor and thus the voltage output. Radiation increases the flux through the sensor, but also results in increased cooling at the surface.

Temperature drop due to contact resistance from the plate heater to the base of the sensor was estimated as 5% of ΔT_{flow}. Temperature drop across the sensor was estimated using 1-D conduction with known sensor thermal conductivity and thickness. Surface temperature and resulting flux (convection plus radiation) were iterated for each data point to find the estimated actual sensor flux and resulting responsivity in Table 3, column 5. The average responsivity is seen to increase by 20%, but is still well below the manufacturer calibration. This calibration based on actual sensor flux shows that the sensor performs differently in the manufacturer's radiation calibration environment than the NIST convection environment.

It may be concluded that the calibration coefficient of this sensor is very sensitive to its mounting and the applied flux—convective versus radiative as well as magnitude. If the sensor were installed in a different environment (e.g. high radiation or low thermal conductivity substrate) it can be anticipated that the calibration would change significantly. These factors will be seen more clearly in the numerical analysis.

Flat Sensor Calibration

The flat sensor was delivered to NIST with a calibration done in conduction (i.e. versus the actual flux passing through the sensor in a known one dimensional heat transfer system) of 4.05 $^{mV}/_{W/cm2}$ at room temperature (responsivity is given as a function of temperature). The

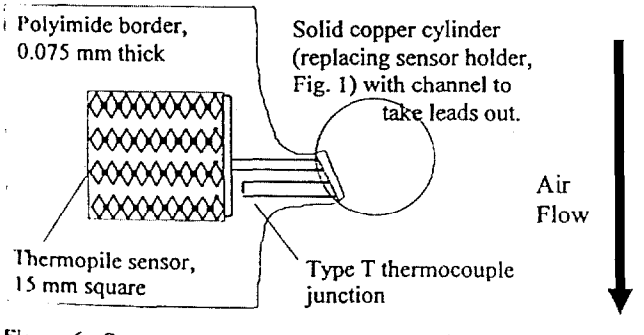

Figure 6: Sensor and mounting relative to 12.7 mm diameter hole in center of convection calibration plate (top view).

0.075 mm thick polyimide sensor has a thermal conductivity of 0.14 W/mK and an estimated emissivity across the IR spectrum of 0.6 (Touloukian and DeWitt, 1970).

Convection calibration of the sensor was performed with the sensor affixed to the surface of the copper calibration plate using a 0.05 mm thick wax sheet, cut to size and melted in place. A border was left on the upstream edge to allow boundary layer recovery before reaching the sensor active area, and the sensor center was located at the same downstream distance as the reference center, Fig. 6. Four calibration points were taken, with results presented in Table 4. Sensor output is linearized by the manufacturer supplied temperature correction function. Despite the temperature correction, the responsivity is still seen to increase with temperature.

As with sensor the plug and button sensors, radiation and conduction issues have been considered. There is no contact resistance problem with the S3 installation, only a temperature drop due to the sensor thermal conductivity (including wax layer) and radiation component (8 % of total flux at ΔT_{flow} = 80).

While the sensor is very thin, the low thermal conductivity limits conduction relative to the copper plate resulting in a surface temperature drop of 3 C at the ΔT_{flow} = 80 C set point. This temperature drop reduces the convective flux from the sensor by 4 %. In addition to this, the higher emissivity of the sensor relative to the reference results in a steadily increasing radiant flux as ΔT_{flow} increases. Accounting for these factors gives the responsivity based on estimated actual sensor flux (Table 4, col. 5).

The sensor average responsivity is now seen to agree well with the manufacturer calibration, although there is still a significant change with temperature. Despite this sensor's very low thermal conductivity (less than that of the button sensor), its very thin design allows for 1-D heat transfer through the sensor, and accurate reporting of the convective flux using the manufacturer calibration if sensor emissivity and thermal conductivity are taken into account.

NUMERICAL MODELING OF SENSORS

Numerical modeling was performed using a commercially available finite differencing thermal analysis code. The final model geometry, Fig. 7, is a 90° pie slice with the center of the sensor modeled with rectangular elements transitioning to wedges at the sensor perimeter. Radiation to the substrate and sensor upper surfaces is assumed to emanate from an isothermal environment. Convection is applied assuming a constant convection coefficient, h. A constant temperature boundary condition on the bottom surface of the model and an adiabatic side condition are used in all cases. Three sensor types were modeled, approximating the three test sensors. All three sensors were modeled as cylinders of uniform thermal conductivity

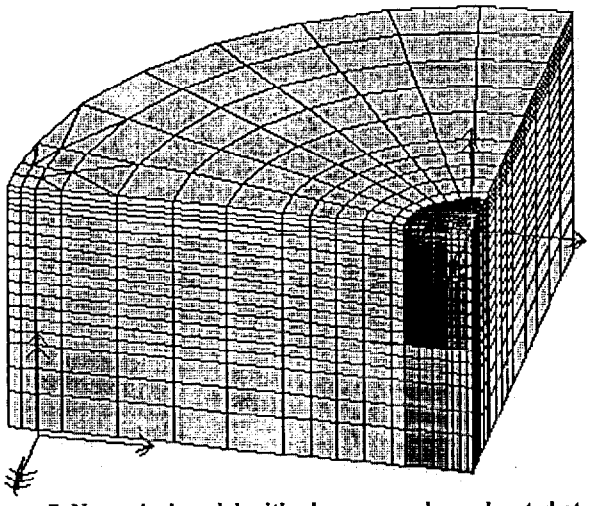

Figure 7 Numerical model with plug sensor shown located at center. Substrate flux is measured across upper brick, left side. Air gap surrounding the sensor is too thin to see in this view.

and 1 cm diameter, mounted in (or on) a substrate of uniform thermal conductivity.

Several calibration constants were considered. In each case, the calibration constant is presented as *actual flux* (undisturbed, desired value) divided by *sensor flux* (conduction through sensor body) giving units of *flux/flux*. The sensor flux was determined by measuring ΔT between two nodes along the centerline of the sensor model, so that $q''_{sens} = k \cdot \Delta T/x$, where x is the vertical distance between the nodes and k is the sensor conductivity. Only the flux along the centerline was considered assuming the active area of the sensors is limited to the central region of the sensor body.

The first calibration of interest is that of incident radiation, $q''_{inc\ rad} = \sigma T_{source}^4$, versus sensor flux. This is very often the calibration shipped with a commercial gage if the expected use of the gage is to measure incident radiation. Correcting for reflected and emitted radiation (Fig. 3) produces a net absorbed flux calibration, $q''_{abs\ rad} = \varepsilon_{sens}\ \sigma (T_{source}^4 - T_{sens}^4)$, although the emitted component (T_{sens}) is typically neglected. This calibration would be shipped with a sensor if the intended use is to measure the actual flux through a surface. A third calibration constant is that found in a convection calibration, where the applied flux is completely convective, $q''_{conv} = h\ \Delta T_{flow}$. Use of these three calibration constants gives insight into sensor performance.

Sensor properties and geometry are given in Table 5. The plug sensor is modeled as an aluminum cylinder mounted in a hole in the substrate, with air beneath the sensor and an air gap of 0.025 mm separating the sensor from the substrate on the side. The temperature difference used to calculate sensor flux was taken between the surface node and a node 0.5 mm below the surface. This approximates the location of the plug sensor differential thermopile. The button sensor

Table 5 Modeled sensor properties

Sensor	*Depth (mm)*	*Sensor material*	*k (W/mK)*	*Sensor emiss.*	*Mounting*
Plug	10	Al	200	0.94	Air gap on sides, air pocket below
Button	3	polymer	0.4	0.94	Potted with epoxy into substrate
Flat	0.075	polyimide	0.14	0.6	Attached with polymer adhesive

is modeled as a 3 mm thick disk of polymer set into the substrate, surrounded by a 0.025 mm gap filled with epoxy. The temperature difference used for sensor flux was taken between a node 1 mm below the surface and a second node 1 mm below that, or the central region of the sensor, again similar to the actual sensor. The flat sensor is modeled as a polyimide disk 0.075 mm thick attached to the substrate surface with a polymer layer 0.025 mm thick. The temperature difference used for sensor flux was taken across the central 0.025 mm of the sensor's thickness.

Numerical radiation calibration was performed with these sensors mounted in/on a copper substrate and exposed to radiation, allowing the system to reach steady state. Convection calibration was done with the same configuration, but with a convective flux boundary condition on the top surface. A summary of these calibration environments is presented in Table 6. Because of the lower conductivity of the button and flat sensors, a lower radiation source temperature was used to minimize sensor heating. The calibration coefficient changes as a function of sensor temperature with respect to substrate temperature.

Calibration results for the three sensors are presented in Table 7. The *Surface temps* columns show the potential mismatch of sensor and substrate temperatures due to several factors: emissivity, thermal conductivity, and contact resistance. A calibration is most useful when the temperature difference in application equals that in calibration. Five fluxes are given in the *Heat flux quantities* columns. Both sensor and substrate fluxes are based on conduction in the numerical model equal to $k \cdot \Delta T/x$, where k is the thermal conductivity (of sensor or substrate), and the temperature difference is taken between two nodes separated vertically by a distance x. The substrate flux is measured between the surface node and that below taken at the perimeter of the model farthest from the sensor (left side, Fig. 7). The incident and absorbed radiation fluxes are as defined previously. The convective flux is taken as that to the substrate, rather than the sensor, fundamentally because the undisturbed flux is the desired flux. The large differences in these fluxes are due to emissivity and thermal conductivity differences, as well as applied convection versus radiation.

The *Calibration coefficients* columns show significant variation among the coefficients from the ideal value of 1.00. The incident radiation coefficients are considerably above one due to emissivity less than unity, as well as to significant re-radiation for the *button* and *flat* sensors where radiation source temperature is lower. The absorbed

Table 6 Calibration environments

Environment	*Substrate material*	*Substrate k (W/mK)*	*Substrate emissivity*	*T_{source}, radiation (°C)*	*T_{amb}, conv (°C)*	*heat transfer coeff. h (W/m^2K)*
Radiation calibration	Cu	400	0.02	1000 (S1), 300 (S2, S3)	25	0
Convection calibration	Cu	400	0.02	----	125	60

Table 7 Numerical modeling results

	Environ-ment	*Surface temps*		*Heat flux quantities*					*Calibration coefficients*		
		T_{sens} (°C)	T_{sub} (°C)	q''_{sens} (kW/m^2)	q''_{sub} (kW/m^2)	$q''_{inc\ rad}$ (kW/m^2)	$q''_{abs\ rad}$ (kW/m^2)	$q''_{conv\ @\ substrate}$ (kW/m^2)	$C_{inc\ rad}$ ($q''_{inc\ rad}/q''_{sens}$)	$C_{abs\ rad}$ ($q''_{abs\ rad}/q''_{sens}$)	C_{conv} (q''_{conv}/q''_{sens})
Plug	Rad cal	56.7	25.21	136	3.03	149.0	139	0	**1.097**	**1.026**	---
	Conv cal	26.7	25.30	5.76	5.98	0	0	5.98	---	---	**1.038**
Button	Rad cal	55.0	25.00	3.86	0.11	6.12	5.13	0	**1.584**	**1.328**	---
	Conv cal	51.5	25.19	3.42	5.99	0	0	5.99	---	---	**1.752**
Flat	Rad cal	27.1	25.00	3.39	0.11	6.12	3.39	0	**1.803**	**1.000**	---
	Conv cal	28.6	25.15	5.78	6.00	0	0	5.99	---	---	**1.036**

radiation and convection calibrations show good agreement for the *plug* and *flat* sensors, all within several percent indicating that the sensors are not sensitive to lateral flux. This agreement confirms real sensor calibration data presented earlier. For the *button* sensor, however, calibration coefficients (Table 7) vary considerably due to different conduction flow paths through the sensor. The differences (1.328 for absorbed radiation versus 1.752 for convection) are similar in magnitude to those observed for the real calibrations of the *button* sensor (manufacturer radiation calibration versus convective calibration).

CONCLUSIONS

Convection calibration data and numerical modeling results demonstrate that calibration coefficients are sensitive to the following parameters: sensor mounting, type of applied flux (convection versus radiation), magnitude of applied flux, contact resistance, properties (k, ε) of sensor relative to substrate, and internal sensor construction (where temperature difference is measured for q''_{sens}). A real sensor will be sensitive to other variables not modeled here (e.g. boundary layer disturbance, radiation spectrum and view angle considerations, and sensor internal construction details). This means that the same sensor can have widely different calibration coefficients depending on the calibration set-up. If these are not matched in application, error in measurement will result. For this reason, ***in situ*** sensor calibration is always desired if possible, and careful sensor design to minimize sensitivity to various unknowns is required.

The generally good performance of sensors S1 and S3 in the convective calibration tests relative to the manufacturer supplied calibrations is confirmed by the numerical modeling. Likewise, for sensor S2, the potential for disagreement from calibration to calibration and from calibration to application is confirmed as well. Analysis of the sensor calibrations shows that correction of sensor measurements can be made to find the flux at the substrate if sensor and substrate properties are known, including sensor and substrate surface temperature.

It may be concluded that the most accurate heat flux measurements are made with a thin differential temperature measurement made at the surface of a sensor body, and with a sensor body that is matched in material and surface properties with the surrounding substrate and mounted with minimal contact resistance. With care in matching calibration to application, small measurement uncertainties are achievable.

ACKNOWLEDGEMENTS

The willingness of heat flux sensor manufacturers to supply sensors is appreciated. Likewise, the lead author would like to acknowledge both NIST and specifically Dr. William Grosshandler of the Building Fire Research Lab, Fire Sensing Group Leader, for their support, and the National Research Council that has sponsored the lead0 author's post-doctoral work at NIST.

REFERENCES

Diller, T.E., 1993, "Advances in Heat Flux Measurements," Advances in Heat Transfer, v.23, Academic Press, Boston.

Diller, T. E., 1998, "Heat Flux," Ch. 6.3 In The Measurement, Instrumentation and Sensors Handbook, Ed. J. G. Webster, CRC Press, Boca Raton, Florida.

Grosshandler, W.L., Blackburn, D., 1997, "Development of a High Conduction Calibration Apparatus," HTD-Vol. 353, Proceedings of the ASME Heat Transfer Division, Vol. 3, pp.153-158.

Holmberg, D.G., Womeldorf, C.A., 1998, "Report on the First-Generation NIST Convective Heat Flux Calibration Facility," NIST Internal Report 6197.

Holmberg, D.G., Womeldorf, C.A., 1999, "A Progress Report on the NIST Convective Heat Flux Calibration Facility," Paper AJTE99-6153, Proceedings of the 5th ASME/JSME Joint Thermal Engineering Conference, Mar 15-20, San Diego, CA.

Keltner, N.R., 1997, "Heat Flux Measurements: Theory and Applications," Ch. 8, In K. Azar (ed.), Thermal Measurements in Electronics Cooling, Boca Raton: CRC Press, 273-320.

Kidd, C.T., Nelson, C.G., 1995, "How the Schmidt-Boelter Gage Really Works," Proceedings of the 41st International Instrumentation Symposium, ISA, Denver, CO, May 7-11, 1995.

Kim, J., Ross, R.A., Dunn, M.G., 1996, "Numerical Investigation of the Heat-Island Effect for Button-Type, Transient, Heat-Flux Gage Measurements," Proceedings of the 1996 National HT Conference, Houston, TX.

Murthy, A.V., Tsai, B.K., Saunders, R.D., 1997, "Radiative Calibrations of Heat Flux Sensors at NIST-An Overview," HTD-Vol. 353, Proceedings of the ASME Heat Transfer Division, Vol. 3, pp.159-164.

Touloukian, Y.S. and DeWitt, D.P., 1970, "Thermophysical Properties of Matter", TPRC Data Series, V.7: Thermal Radiative Properties, IFI/Plenum, NY.